International Journal of Pharmaceutics 623 (2022) 121884

Contents lists available at ScienceDirect

International Journal of Pharmaceutics

journal homepage: www.elsevier.com/locate/ijpharm

Colon-targeted oral nanoparticles based on ROS-scavenging hydroxyethyl starch-curcumin conjugates for efficient inflammatory bowel disease therapy

Chenlan Xu [a,1], Shuting Chen [a,1], Cuiping Chen [a], Yangcan Ming [c], Jiahao Du [a], Jinyi Mu [a], Fang Luo [a,b], Da Huang [a,*], Na Wang [c,*], Zhenyu Lin [b], Zuquan Weng [a,b,*]

[a] College of Biological Science and Engineering, Fuzhou University, Fuzhou, Fujian 350108, China
[b] Ministry of Education Key Laboratory for Analytical Science of Food Safety and Biology, Fujian Provincial Key Laboratory of Analysis and Detection for Food Safety, College of Chemistry, Fuzhou University, Fuzhou, Fujian 350108, China
[c] Department of Pediatrics, Wuhan NO.1 Hospital, Wuhan, Hubei 430022, China

ARTICLE INFO

Keywords:
Oral nanoparticles
Inflammatory bowel disease
Anti-inflammatory
ROS-scavenging
Targeted delivery
Combination therapy

ABSTRACT

Co-delivery of anti-inflammatory drugs and reactive oxygen species (ROS) scavengers by stimuli-responsive oral nanoparticles is deemed to be a favorable strategy for inflammatory bowel disease (IBD) therapy. In this study, using micelles formed by CUR conjugated hydroxyethyl starch (HES) as vehicles, dexamethasone (DEX)-loaded HES-CUR nanoparticles (DHC NPs) with desirable size, negative surface charge, good stability in the harsh gastric environment, and excellent ROS scavenging activity are developed as a colon-targeted oral formulation for treating IBD. Due to the degradation of HES in response to α-amylase overexpressed in the inflamed colon, the DHC NPs release drugs in an α-amylase-responsive manner. Meanwhile, the DHC NPs can be effectively internalized by macrophages and show excellent cytocompatibility with macrophages since they are composed of food-derived compounds. Importantly, *in vivo* studies reveal that the DHC NPs are capable of targeting the inflamed colon induced by dextran sulfate sodium (DSS), and the targeted and combination therapy enhances the efficacy of free DEX and significantly relieves the impairment caused by DSS-induced ulcerative colitis. Incorporating the merits of targeted drug delivery and combined therapy with an anti-inflammatory drug and ROS scavenger, the DHC NPs are promising for developing novel oral formulations for IBD therapy.

1. Introduction

Inflammatory bowel disease (IBD), a chronic, relapsing-remitting, and multifactorial inflammatory disorder of the gastrointestinal tract, is clinically manifested in the forms of ulcerative colitis (UC) and Crohn's disease (CD) (Abraham and Cho, 2009). UC is characterized by inflammation of the colonic mucosa, with a continuous and segmental distribution, extending from the proximal colon to the rectum, while CD is a transmural, non-continuous layer inflammation that develops along the whole GIT, most commonly the terminal ileum or the perianal region (Guan, 2019). The prevalence of UC and CD in developed countries is higher than 0.3% and their morbidity continues to increase sharply in newly industrialized countries (Ng et al., 2017). Typically, the clinical presentation consists of abdominal pain, diarrhea, rectal bleeding, general fatigue, and weight loss. Besides, IBD predisposed patients have a high incidence of developing various complications and other conditions, such as stenosis, fistula, and colitis-associated cancer, which often lead to high mortality (Kotla et al., 2018; Graham and Xavier, 2020). Currently, there is no complete cure for IBD. Clinically, immunosuppressants and anti-inflammatory drugs including aminosalicylates, and glucocorticoids are mostly prescribed for IBD therapy (Jeong et al., 2019).

Anti-inflammatory glucocorticoids such as dexamethasone (DEX), budesonide, and betamethasone are commonly used for severe IBD because they can down-modulate innate and adaptive immune cell activation (Seshadri et al., 2018). Unfortunately, long-term systemic

* Corresponding authors at: 2 Xueyuan Road, College Town, Fuzhou, Fujian 350108, China (D. Huang and Z. Weng) 215 Zhongshan Road, Qiaokou District, Wuhan, Hubei 430022, China (N. Wang).
E-mail addresses: huangda@fzu.edu.cn (D. Huang), wangna1027@126.com (N. Wang), zqweng@fzu.edu.cn (Z. Weng).
[1] These authors contributed equally to this work.

https://doi.org/10.1016/j.ijpharm.2022.121884
Received 9 February 2022; Received in revised form 9 May 2022; Accepted 29 May 2022
Available online 2 June 2022

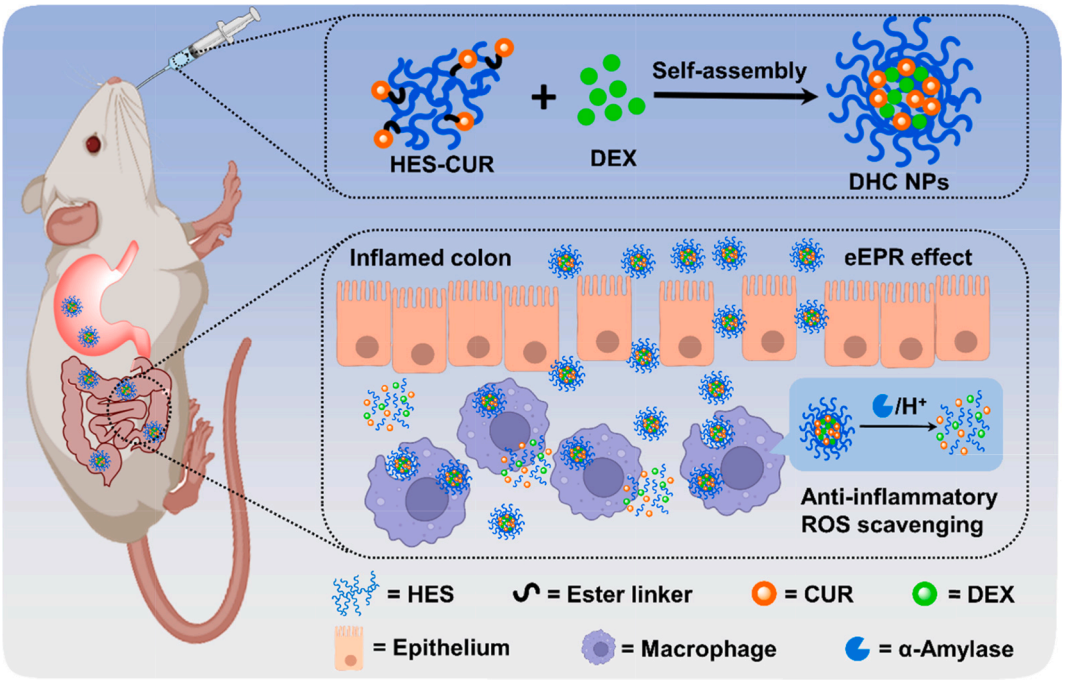

Fig. 1. Schematic illustration of fabrication and oral drug delivery process of DHC NPs.

administration of glucocorticoids is usually associated with extra-intestinal manifestations and complications, such as hypertension, diabetes, low bone mass, and osteoporosis (Sood et al., 2002). Instead of systemic administration, recent studies focus on the strategies for delivering drugs to the inflammatory site explicitly by employing nanoparticles-based oral formulations due to the epithelial enhanced permeation and retention effect (eEPR) in inflammatory tissues (Kesharwani et al., 2018; Zai et al., 2018; Dou et al., 2020; Nguyen et al., 2021). The loss of intercellular junctions between endothelial cells leads to leaky and unstable nascent vascular networks in inflamed tissues, thus nanoparticles can passively target the inflammatory sites (Gou et al., 2019). In addition, it was reported that nanoparticles are capable of penetrating the mucus layer in the bowel deeply (Le et al., 2021). Furthermore, the microenvironment of IBD is associated with pathophysiological characteristics such as high levels of reactive oxygen species (ROS), lower pH, overexpressed enzymes (α-amylase, neutrophil elastase, myeloperoxidase, etc.) (Kotla et al., 2018; Bertoni et al., 2018; Hua et al., 2015; Zhang et al., 2020; Fousekis et al., 2018; Castangia et al., 2015). Therefore, nanoparticles, especially stimuli-responsive nanoparticles are promising vehicles for targeted drug delivery in IBD treatment. Ali et al. reported budesonide-loaded poly(lactic-co-glycolic) acid nanoparticles with a pH-sensitive coating for improved mucosal targeting in IBD therapy (Ali et al., 2014). Wang et al. developed DEX-loaded esterase-responsive nanovesicles based on poloxamer and the co-delivery of DEX and tannic acid achieved combined treatment of IBD (Wang et al., 2018). However, most of these nanoparticles were based on synthetic materials which arouse safety concerns, and the carriers themselves lack pharmacological activity.

Recently, the use of natural product-based therapies for the treatment of IBD has increased substantially owing to the broad range of beneficial biological activities and excellent biosafety (Debnath et al., 2013). Particularly, it was reported the combination of anti-inflammatory drugs and natural polyphenols with ROS scavenging activity could achieve a better therapeutic effect for IBD because excess ROS is involved in the initiation and progression of IBD (Liu et al., 2020). Curcumin (CUR), an active hydrophobic polyphenol derived from the perennial herb Curcuma longa, has been identified as one of the most active natural polyphenols for IBD due to its effective antioxidant and anti-inflammatory activity both *in vivo* and *in vitro* (Vecchi Brumatti et al., 2014; Gao et al., 2021). IBD is generally characterized by the upregulation of cytokines presented inside the intestinal lumen, activated through various inflammatory cascades, and associated with oxidative stress (Friedrich et al., 2019). Ajaikumar B et al. summarized the therapeutic potentials of CUR including reduction of tissue damage and oxidative stress, cytokine expression modulation, and suppression of inflammation-related gene expression. Apart from inhibiting activation of transcriptional factors, multiple protein kinases, and anti-apoptotic proteins, CUR was also found to modulate various inflammatory cytokines, through the suppression of inflammatory transcription factor NF-κB (Kunnumakkara et al., 2008). In addition, gut health and permeability change significantly because of the interaction between CUR and intestinal microbes (Pluta et al., 2020). It has been found that CUR transforms into tetrahydrocurcumin by the enzymatic activity of *Escherichia coli*, which affects intestinal permeability (Hassaninasab et al., 2011). Yasuyuki Deguchi has demonstrated that CUR, as a nontoxic natural dietary product, could be beneficial in the therapeutic strategy for IBD patients (Deguchi et al., 2007). Therefore, we hypothesized that co-delivery of CUR and anti-inflammatory drugs such as DEX using stimuli-responsive nanoparticles may achieve a remarkable curative effect for IBD. However, oral nanoparticles capable of co-delivering DEX and CUR haven't been developed and their therapeutic effect against IBD remains unknown.

Previously, we reported the fabrication of polymeric micelles by conjugating CUR to food-derived hydroxyethyl starch (HES) *via* a cleavable ester linker and self-assembly of the obtained HES-CUR conjugates (Chen et al., 2020). The polymeric micelles exhibited excellent stability, biocompatibility, acid-responsive behavior, and significantly enhanced the ROS scavenging activity and bioavailability of CUR by increasing the solubility of CUR in water. Herein, we further utilized these polymeric micelles to encapsulate anti-inflammatory drug DEX and fabricated DEX-loaded HES-CUR nanoparticles (DHC NPs) as an oral nanomedicine for IBD therapy. As illustrated in Fig. 1, the orally administered DHC NPs can accumulate in the inflamed colons via the eEPR effect and then be internalized by macrophages. Subsequently, the α-amylase in the colon or the acidic environment in lysosome/endosome will trigger the release of loaded drugs and achieve the therapeutic effect

by anti-inflammation and ROS scavenging. The morphology, zeta potential, drug-loading capacity, biocompatibility, intracellular ROS scavenging activity of the DHC NPs, as well as cellular uptake by macrophages were characterized. The oral delivery process was simulated in the environment of gastric and intestinal fluid to demonstrate the stability and drug release behavior of the combined drug delivery system. We also evaluated the potential of this novel oral nanomedicine in IBD therapy by investigating the targeting effect to inflamed colon and the therapeutic effect against dextran sulfate sodium (DSS)-induced UC in mice.

2. Materials and methods

2.1. Materials

DEX (98%), 2,2-diphenyl-1-picrylhydrazyl (DPPH, 97%), thiazolyl blue tetrazolium bromide (MTT), paraformaldehyde (99%), and 4′,6-diamidino-2-phenylindole dihydrochloride (DAPI, 98%) were purchased from Aladdin Industrial Corporation (Shanghai, China) and used as received. Lipopolysaccharide (LPS) and 2′,7′-dichlorofluorescein diacetate (DCFDA) were purchased from Beyotime Biotechnology (Shanghai, China). Rhodamine phalloidin (RP) was purchased from ABclonal Inc. (Woburn, Maryland, USA). Dextran sulfate sodium (DSS, colitis grade, molecular weight 360 ~ 500 kDa) was purchased from MP Biomedicals (Santa Ana, California, USA). Near-infrared dye IR780 (99%) was obtained from Energy Chemical (Shanghai, China). Dulbecco's modified Eagle medium (DMEM) and fetal bovine serum (FBS) were purchased from Gibco. HES-CUR was synthesized following our previous report (Chen et al., 2020). All other reagents were analytical grade and used directly.

2.2. Preparation and characterization of DHC NPs

HES-CUR conjugate and HES-CUR NPs (HC NPs) were prepared as previously described (Chen et al., 2020). To prepare the DHC NPs, HES-CUR conjugate (10 mg) and DEX (0.5 or 1 mg) were dissolved in 500 μL of DMSO and the solution was slowly injected into 1 mL of ultrapure water under stirring through a syringe pump within 20 min. After dialysis against ultra-pure water for 6 h (MWCO: 3500 Da) and centrifugation (10000 rpm, 3 min) to remove the organic solvent and excessive DEX, the DHC NPs solution was obtained for further experiments. Using a similar method, IR780 loaded HES-CUR NPs (IHC NPs) were prepared for the biodistribution analysis.

The morphology of DHC NPs was observed by transmission electron microscopy (TEM, HT7700, Hitachi, Japan) after the samples were negatively stained by 2 wt% sodium phosphotungstate. The hydrodynamic average sizes and zeta potentials were assessed by dynamic light scattering (DLS) using a zetasizer (Nano-ZS, Malvern, UK).

2.3. Determination of drug loading and encapsulation efficiency of DEX in DHC NPs

A certain amount of freeze-dried DHC NPs was dispersed in a certain volume of methanol solution and the solution was sonicated at 37 °C for 10 min to release DEX completely. The concentration of DEX in the solution was detected by high performance liquid chromatography (HPLC, Thermo Ultimate 3000, USA) with a detection wavelength of 240 nm and a mixture of methanol and ultra-pure water (7:3, v/v) was used as the mobile phase at a flow rate of 1.00 mL/min. The drug loading efficiency (DLE) and encapsulation efficiency (EE) were calculated using the following equation:

$$DLE(\%) = \frac{C_{DEX}V}{M_{DHCNPs}} \times 100\%$$

$$EE(\%) = \frac{C_{DEX}V}{M_{DEX}} \times 100\%$$

Where $C_{DEX}V$ is the amount of DEX recovered, $M_{DHC\ NPS}$ is the amount of DHC NPs, M_{DEX} is the amount of initially fed DEX.

2.4. Stability of DHC NPs in gastrointestinal simulations

The stability of DHC NPs in simulated gastric fluid (SGF, pH 1.2) and simulated intestinal fluid (SIF, pH 6.8) with α-amylase (0.064 KNU/mL) was investigated by monitoring the variation of size of the DHC NPs in these solutions. Specifically, the freeze-dried DHC NPs powder was dispersed in SGF and SIF containing α-amylase with a concentration of 1 mg/mL, respectively. The solutions were incubated at 37 °C in a shaker (100 rpm) and the hydrodynamic size of the DHC NPs was measured by DLS at predetermined intervals. The stability of DHC NPs in SGF and SIF was monitored for 4 h and 20 h respectively.

2.5. In vitro release of DEX from DHC NPs

Following the previous report (Wang et al., 2018), the *in vitro* release profile of DEX from DHC NPs was evaluated in simulated gastric fluid (SGF, pH 1.2) and simulated intestinal fluid (SIF, pH 6.8). SGF was used as release medium for the first 4 h and then SIF with or without α-amylase (0.064 KNU/mL) was used as release medium for the following 20 h, respectively. A series of DHC NPs solutions with equivalent DEX concentration were prepared by dispersing the freeze-dried DHC NPs powder in the releasing medium (the final concentration of DEX is 109 μg/mL). Then the samples were incubated at 37 °C in a shaker (100 rpm). Three samples were taken out at predetermined intervals and the DEX concentration in the samples was measured by HPLC. The cumulative release rate (%) of DEX was calculated according to the following formula:

$$Cumulative\ release(\%) = \frac{C_t V}{m_{DEX}} \times 100\%$$

where C_t is the concentration of released DEX after t hours, V is the volume of release medium, and m_{DEX} is the total mass of DEX in the DHC NPs.

2.6. In vitro DPPH radical scavenging assay

200 μL of DPPH solution (0.04 mM) in ethanol was added to the 96-well plate, then the HC NPs and DHC NPs dispersed in 20 μL of ultrapure water were added to make the final DHC NPs concentration be 0 ~ 1000 μg/mL. The solutions were then incubated in the dark for 30 min at room temperature, and the absorbance of the solution was measured at 517 nm with a microplate reader (BioTek, Synergy H1, USA). DPPH inhibition rate was calculated according to the following formula:

$$DPPH\ inhibition(\%) = \frac{A_c - A_e}{A_c} \times 100\%$$

Where A_c is the absorbance of the control (no sample, only DPPH), and A_e is the absorbance of the solution treated with NPs. Each experiment was repeated three times.

2.7. In vitro cellular uptake

Macrophage RAW 264.7 were incubated in DMEM supplemented with 10% FBS and 1 wt% penicillin/streptomycin at 37 °C in a 5% CO_2 incubator for 2 or 3 days. When the cells reached a confluence of about 80%, 1 mL of trypsin solution was added to detach the cells. The cells were gently blown with a pipette to form cell suspension, which was then centrifuged to collect the cells. Subsequently, an appropriate amount of fresh culture medium was added to form a cell suspension with a density of 2×10^5 /mL, and 1 mL of cell suspension was seeded in the glass-bottomed confocal culture dish.

After incubation for 24 h, the medium was removed and fresh mediums containing DHC NPs (0.2 mg/mL) were added. After incubation for 2 and 12 h respectively, the medium was removed, the cells were washed with PBS (2 mL, pH 7.4) for 3 times, and then fixed with 4% paraformaldehyde for 10 min. The cells were then washed with PBS for 3 times and treated with RP for 30 min and DAPI (1.0 μg/mL) for 15 min in sequence to label the cytoskeleton and nuclei respectively. Finally, the cells were washed with PBS for 3 times again and fixed on the culture

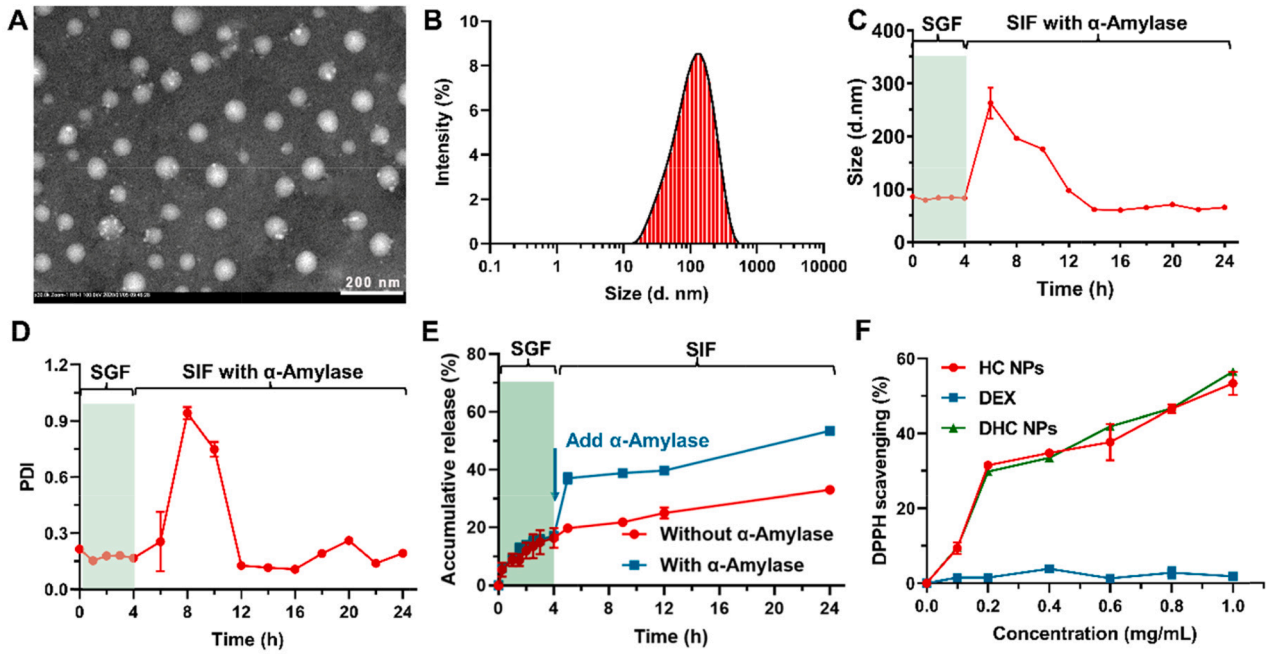

Fig. 2. Morphology and physicochemical properties of DHC NPs. (A) Representative TEM image of DHC NPs. (B) Size distributions of DHC NPs determined by DLS. The variation of (C) size and (D) PDI of DHC NPs in SGF and SIF with α-amylase. (E) *In vitro* release of DEX from the DHC NPs in SGF and SIF. (F) DPPH radical scavenging activity of HC NPs, DEX, and DHC NPs.

dish. The localization of DHC NPs in raw 264.7 cells was monitored by confocal laser scanning microscopy (CLSM, Nikon Eclipse TE2000, Japan) using FITC channel (excited at 488 nm).

The cellular uptake was also analyzed using flow cytometry. After incubated with DHC NPs (0.2 mg/mL) for 2 and 12 h respectively, the medium was removed, and the cells were harvested with trypsin by centrifugation and then resuspended in PBS. The cell suspension was analyzed on a flow cytometer (BD Accuri C6 plus, USA) and the intensity of FITC channel was used to indicate the internalization of DHC NPs.

2.8. Cytotoxicity assay

The biocompatibility of HC NPs and DHC NPs was evaluated by MTT assay using macrophage RAW 264.7 as a model cell. The cells were seeded in 96-well plates with a density of 2×10^4 cells per well and incubated for 24 h. Then the medium in each well was replaced with 200 μL of fresh medium containing HC NPs or DHC NPs with a concentration of 200 ~ 1000 μg HES-CUR equiv./mL. After incubation for 24 h, the medium was replaced with 200 μL of fresh medium and 20 μL of MTT was added to each well and followed by incubation for 2 h. Then the medium was removed and 200 μL of DMSO was added to dissolve the blue and purple nail crystals. The absorbance of each well was measured at 570 nm with a microplate reader. Relative cell viability was calculated by comparing the absorbance of the well treated with the sample to that of the negative control.

2.9. Intracellular ROS scavenging of DHC NPs

RAW 264.7 cells were seeded in 96-well plates with a density of 2×10^4 cells per well and incubated for 24 h. Then the medium in each well was replaced with 200 μL of fresh medium containing 100 ng/mL of LPS to stimulate the generation of ROS, except that one group was replaced with 200 μL of fresh medium without LPS. Subsequently, one group of LPS-treated cells didn't receive any treatment, the other groups were treated with CUR (13 μg/mL), HC NPs (100 μg/mL) and DHC NPs (100 μg/mL) respectively. After incubation of 24 h, the medium was discarded and the cells were washed with PBS for 3 times before adding ROS probe DCFDA (10 μM). After incubated in dark for 30 min, the fluorescence emission at 525 nm was detected by a microplate reader at an excitation wavelength of 488 nm to quantify the level of intracellular ROS.

Similarly, RAW 264.7 cells were seeded in glass-bottomed confocal culture dishes with a density of 2×10^5 cells per dish and then treated with the same procedures as mentioned above. After treatment, the nuclei of cells were stained with DAPI (1.0 μg/mL) and ROS probe DCFDA was added to detect the intracellular ROS. The localization and level of intracellular ROS were then monitored by CLSM using FITC channel (excited at 488 nm).

2.10. In vivo studies of the DHC NPs

BALB/c mice (male or female, aged between 8 and 12 weeks) were used in the *in vivo* studies. The mice were housed under SPF conditions and all experiments performed on them comply with the institutional ethics committee and the guidelines for the care and use of laboratory animals of Fuzhou University. UC model was created by replacing the drinking water with DSS solution (3%, w/v) for 7 consecutive days.

2.10.1. Biodistribution

Before the experiments, normal mice or mice with DSS-induced UC (n = 3) were treated with paraffin depilation, fasting, and free water. The next day, 400 μL of IHC NPs suspension (1 mg/mL) was administered by oral gavage. After 3 h, 10 h, and 24 h, the mice were intraperitoneally injected with an anesthetic (5% chloral hydrate, 150 μL), and then fluorescent images of the mice and colons were captured using an *in vivo* near-infrared imaging system (In-Vivo Master, Grand-imaging Technology Co., Ltd, Wuhan, China).

2.10.2. In vivo therapeutic effect against DSS-induced UC

Groups of mice with induced UC (n = 5 for each group) were treated with DEX suspension (2 mg/kg), HC NPs (72 mg/kg), DHC NPs (low dosage, 37 mg/kg) and DHC NPs (high dosage, 74 mg/kg) daily for 5 days via oral gavage. The healthy mice and those received DSS only were used as controls. All mice were examined daily to monitor body weights

and disease activity index (DAI) scores, which were determined from weight loss, stool consistency, and stool bleeding as described in a previous report. After the treatment was ended, the mice were sacrificed by CO_2 euthanasia and the lengths of the colons were measured. Subsequently, the colon segments were fixed in formalin solution and embedded in paraffin. Then the colon samples were sectioned at a thickness of 5 μm and stained with hematoxylin and eosin (H&E) for histological analysis.

2.11. Statistical analysis

Data were presented as mean ± standard deviation (SD). Student's *t*-test was performed to compare the statistical difference between groups, $^*P < 0.05$ was considered to have a significant difference. The plotting was performed using GraphPad Prism 8 software.

3. Results and discussion

3.1. Preparation and characterization of DHC NPs

Our previous studies demonstrated that the amphiphilic HES-CUR conjugate could self-assemble into micellar nanoparticles (HC NPs) with an appropriate hydrophilic/hydrophobic ratio (Chen et al., 2020). As a hydrophobic drug, DEX can be encapsulated in the hydrophobic region of nanoparticles *via* hydrophobic interaction. By adjusting the mass ratio of DEX and HES-CUR, we prepared DHC NPs with different mass ratios of DEX and HES-CUR, named as 5% DHC NPs and 10% DHC NPs respectively. The average particle size, PDI, Zeta potential, DLE, and EE of these NPs were summarized in Table S1. The mean hydrodynamic diameter of 5% DHC NPs and 10% DHC NPs were<100 nm with uniform distribution (Table S1 and Fig. S1). The zeta potential of the 5% DHC NPs and 10% DHC NPs were about −28.0 and −29.4 mV respectively, which will help them to keep stable by electrostatic repulsion. Increasing the feeding ratio of DEX and HES-CUR from 5% to 10% didn't show enhancement of DLE, therefore we chose 5% DHC NPs as the appropriate formulation for the following research, which was referred to as DHC NPs. As shown in Fig. 2A, the DHC NPs are spherical with a size of about 40–60 nm, in accordance with the size determined by DLS (Fig. 2B). The concentration of DEX in the DHC NPs solution is 110 μg/ml, which is 10 times higher than the solubility of DEX in water, indicating the good solubilization effect.

3.2. Stability of DHC NPs in gastrointestinal simulations

The harsh gastric environment is a crucial challenge for oral formulations. A successful oral formulation for IBD should keep stable in

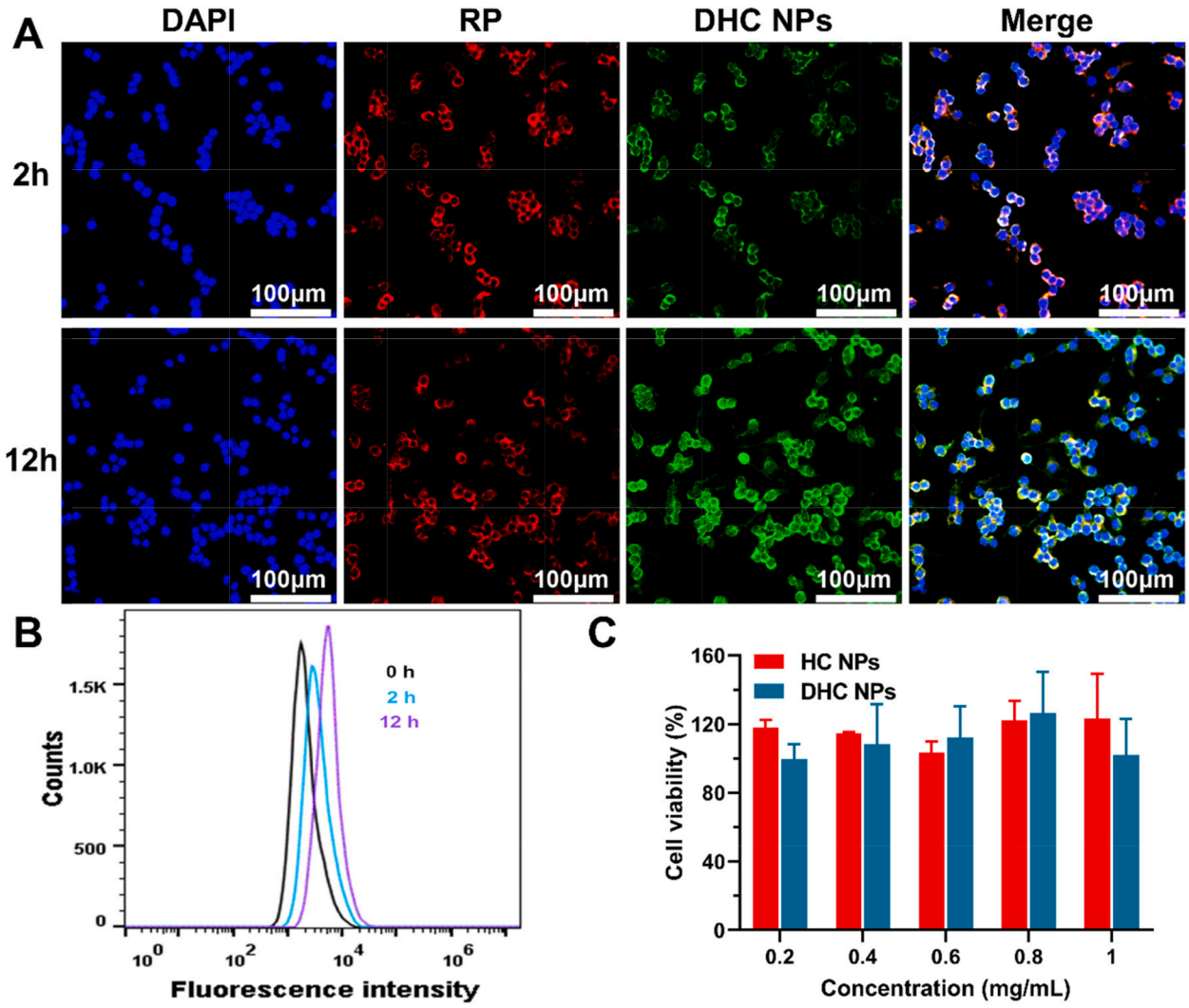

Fig. 3. Cellular uptake and cytotoxicity of DHC NPs against RAW 264.7 cells. (A) CLSM images and (B) fluorescence intensities determined by flow cytometry of RAW 264.7 cells after incubation with DHC NPs for 2 and 12 h. Blue: nuclei; Red: cytoskeleton; Green: DHC NPs. (C) Cell viabilities of RAW 264.7 cells after incubation with HC NPs and DHC NPs for 24 h.

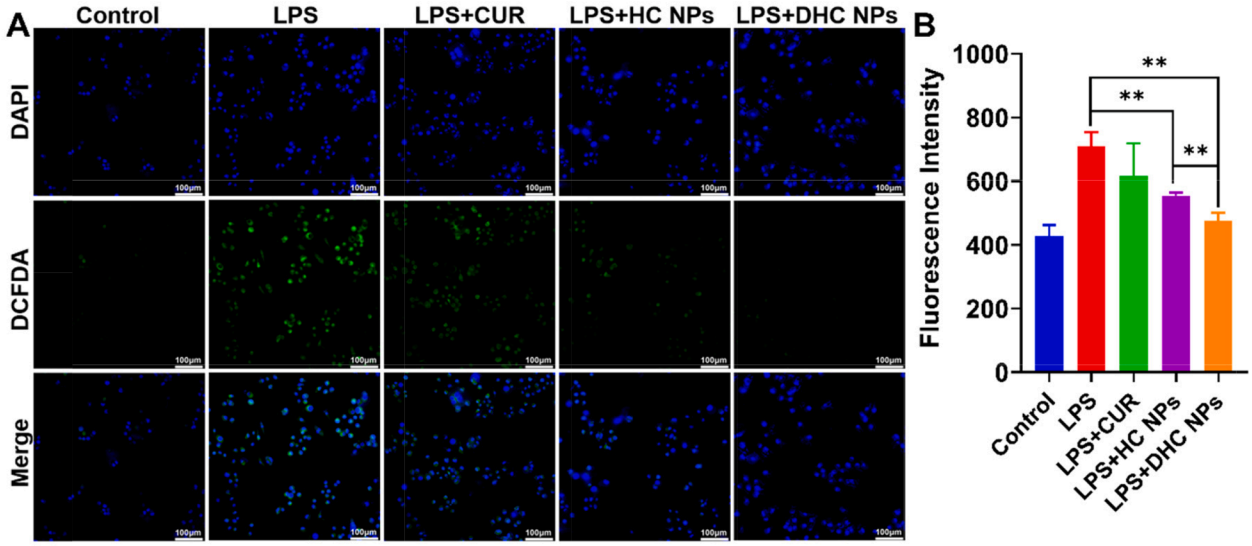

Fig. 4. Intracellular ROS scavenging activity of DHC NPs. (A) CLSM images of RAW 264.7 cells with different treatments. Blue: nuclei; Green: ROS. (B) Fluorescence intensity of DCFDA in RAW 264.7 cells with different treatments. $^{**}P < 0.01$.

the gastric environment and then cleave in the inflamed colon to release payloads. To investigate the stability of the DHC NPs during the oral delivery, the size and PDI of the DHC NPs in SGF and SIF were monitored by DLS. α-Amylase was added to the SIF to mimic the microenvironment of inflamed colon and the stability of DHC NPs was monitored for 4 h and 20 h respectively to simulate the transportation time of orally administered formulations in the human gastrointestinal tract (Camilleri et al., 1989). As shown in Fig. 2C-D, both the size and PDI of the DHC NPs showed negligible variation during the 4 h of incubation in SGF, indicating that the DHC NPs can keep stable during their stay in the harsh gastric environment. The excellent stability of DHC NPs in the acidic SGF is probably ascribed to that the acid-labile ester groups in the HES-CUR conjugates are embedded in the hydrophobic core of the micelles and separated from protons in the SGF. While in the SIF with α-amylase, the size and PDI of DHC NPs increased a lot after 2 ~ 4 h due to the cleavage of the DHC NPs induced by degradation of HES in response to α-amylase and formation of large and heterogeneous aggregates. Subsequently, the size and PDI decreased gradually in the following hours, indicating that the further degradation resulted in small fragments or nanoparticles formed by reassembly of the fragments. These results suggested that the DHC NPs can resist the harsh gastric environment, deliver payloads to the intestinal tract and release payloads in the inflamed colon.

3.3. *In vitro release of DEX from DHC NPs*

In vitro release was carried out at 37 °C in SGF with a pH of 1.2 and SIF with a pH of 6.8 in sequence to simulate the release profile of orally administered formulations. To investigate the α-amylase responsive behavior of the DHC NPs, the release profile in SIF with or without α-amylase was also monitored. Given that the transportation time of orally administered formulations in the human stomach and intestine is about 2–4 h and 12–48 h respectively (Camilleri et al., 1989), the release of DEX from DHC NPs in SGF and SIF was monitored for 4 h and 20 h respectively. Within the first 4 h, DHC NPs released<20% of DEX and only about 30 wt% of DEX released within the next 20 h in α-amylase-free SIF, while the cumulative release of DEX reached more than 50% in the SIF with α-amylase (Fig. 2E). It revealed that the presence of α-amylase accelerated the liberation of DEX from the DHC NPs in contrast to the slow drug release profile in SIF without α-amylase. This α-amylase responsive release manner is not surprised since the HES can be degraded by α-amylase. Besides, our previous study proved that a faintly acidic environment could accelerate the release of CUR from HC NPs since the CUR was attached to HES-CUR conjugates *via* an acid-labile ester bond (Chen et al., 2020). Considering the high level of α-amylase in the intestine of patients with IBD and the lower pH of inflamed tissues, IBD-specific drug delivery can be achieved using the DHC NPs.

3.4. *DPPH scavenging activity of DHC NPs*

Previous studies had reported that CUR has potential anti-inflammatory activity due to the ROS scavenging activity of its two phenolic hydroxyl groups and an enol from a β-diketone moiety (O'Toole et al., 2016; Cunha Neto et al., 2019; Burge et al., 2019). Our previous work verified that HC NPs self-assembled from HES-CUR conjugates enhanced the anti-oxidative activity of CUR owing to the improved solubility, though one phenolic hydroxyl group was sacrificed (Chen et al., 2020). To further examine whether DHC NPs retained the anti-oxidative activity of parent CUR, the ROS scavenging activities of HC NPs, DHC NPs, and DEX were evaluated using DPPH radical scavenging assay. As summarized in Fig. 2F, both DHC NPs and HC NPs showed increased scavenging activity against DPPH radicals with the increase of concentration, while DEX had no scavenging activity on DPPH radicals at all, indicating the loading of DEX didn't affect the excellent anti-oxidative activity of HC NPs.

3.5. *Cellular uptake and cytotoxicity of DHC NPs*

Macrophages in the inflammatory tissues of the colon are the most important targets of drug delivery for IBD therapy (Zhang et al., 2020), hence RAW 264.7 macrophages were chosen as a model cell line for cellular uptake and cytotoxicity investigations. Effective cellular uptake is an important step to implement the function of CUR and DEX. To monitor the internalization of DHC NPs, RAW 264.7 cells were treated with DHC NPs for 2 and 12 h, and the nuclei and cytoskeleton were labeled with DAPI (blue) and RP (red) respectively. Then the location of DHC NPs was tracked by taking advantage of the intrinsic green fluorescence of CUR. As expected, green fluorescence was observed in the cells and overlapped with the red fluorescence area (cytoskeleton) after being cultured with the DHC NPs for 2 h, suggesting the effective internalization of DHC NPs (Fig. 3A). With a longer incubation time, the uptake of DHC NPs increased a lot, which was proved by the stronger green fluorescence. Additionally, the internalization of DHC NPs by

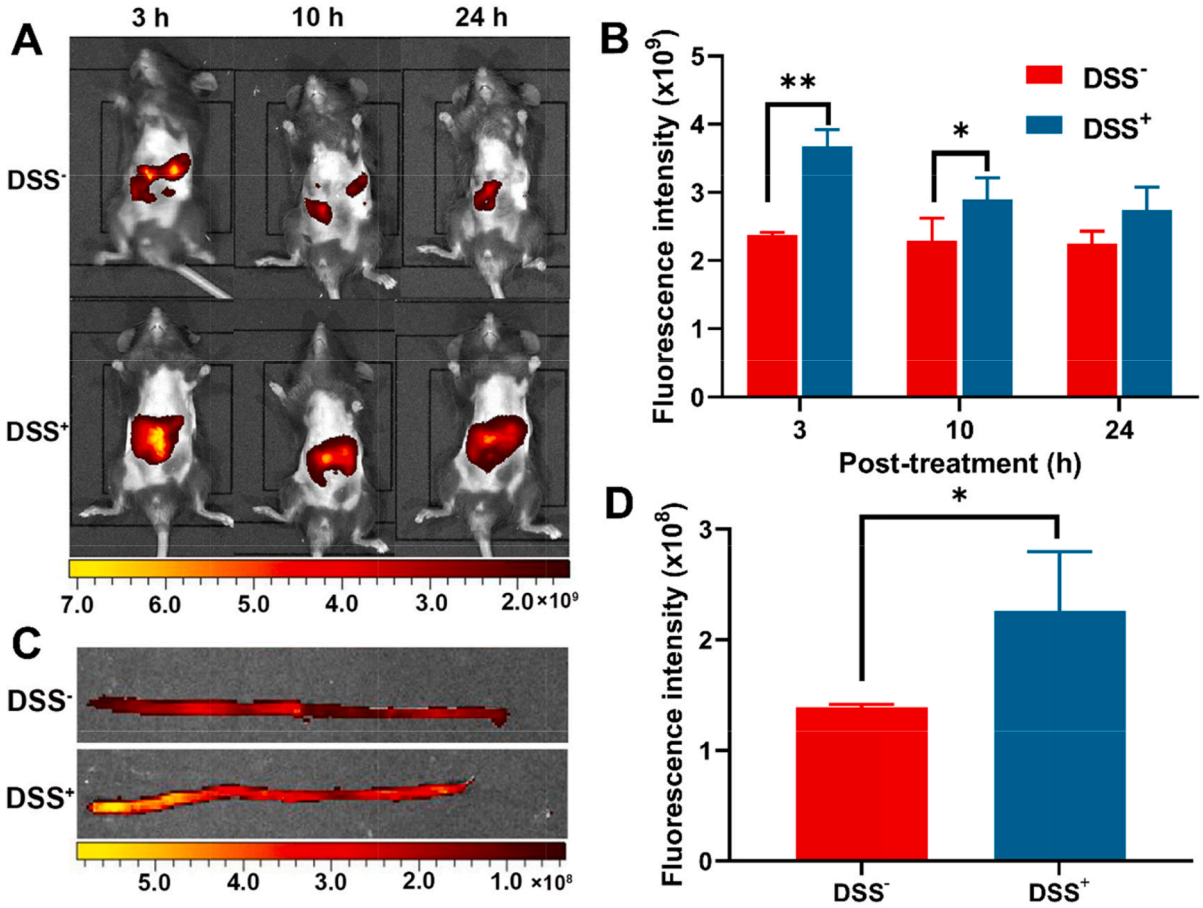

Fig. 5. Biodistribution of IHC NPs in mice with or without DSS-induced UC. (A) Fluorescence images of mice after orally administered IHC NPs for different hours. (B) Quantitative analysis of fluorescence intensities at the regions of interest. (C) Fluorescence images of colons extracted from mice after orally administered IHC NPs for 24 h. (D) Quantitative analysis of fluorescence intensities at the colons. Data is presented by mean ± SD, n = 3, $^{*}P < 0.05$, $^{**}P < 0.01$.

RAW 64.7 was quantified by flow cytometry. As shown in Fig. 3B, the fluorescence intensity enhanced over culture time, which was consistent with the observations on CLSM. It has been reported that HES-based nanoparticles permeated across the cell membrane rapidly by endocytosis (Paleos et al., 2017; Hu et al., 2016), which may explain the time-dependent increase in intracellular uptake of DHC NPs.

As vehicles composed of food-derived compounds, the HC NPs are expected to have excellent biocompatibility. Previously we confirmed that HC NPs were not toxic to human skin fibroblast cells (Chen et al., 2020). In this study, we further investigated the cytotoxicity of HC NPs and DHC NPs against RAW264.7 cells by MTT assay to preliminarily evaluate their biosafety in IBD therapy. As demonstrated in Fig. 3C, the viabilities of cells treated by HC NPs with concentrations ranging from 0.2 to 1 mg/mL were all above 95%. Similar to HC NPs, DHC NPs didn't show toxicity to the RAW264.7 cells even at high concentrations, indicating the loading of DEX didn't cause cytotoxicity to macrophages. The results implied that both HC NPs and DHC NPs have good biosafety in IBD therapy within the applied dose range.

3.6. Intracellular ROS-scavenging activity of DHC NPs

The anti-oxidative activity of the DHC NPs was preliminarily confirmed by the DPPH scavenging assay, but whether the DHC NPs will retain their anti-oxidative activity in the complicated intracellular environment remains unknown. Therefore, we further carried out intracellular ROS-scavenging assays in RAW 264.7 cells to evaluate the intracellular anti-oxidative activity of the DHC NPs. The generation of ROS in the cells was induced by LPS. After treatment with CUR, HC NPs, and DHC NPs, the intracellular ROS level was detected by DCFDA, which is a ROS probe that can only show fluorescence emission after being oxidized by ROS. The successful generation of ROS was confirmed by the bright green fluorescence in the cells treated with LPS, while the cells treated with CUR, HC NPs, and DHC NPs all showed decreases in the green fluorescence at different levels (Fig. 4A), manifesting that the intracellular ROS was scavenged by these formulations. Among the three formulations, DHC NPs demonstrated the best ROS-scavenging effect, which was also confirmed by the quantitative analysis summarized in Fig. 4B. Unlike that the HC NPs and DHC NPs showed similar scavenging activity in the DPPH scavenging assay, the intracellular ROS scavenging activity of DHC NPs is significantly higher than that of HC NPs. This difference can be explained by the different roles DEX played in the two assays. The DPPH scavenging activity of HC NPs and DHC NPs is only attributed to the CUR in these nanoparticles, and DEX showed no effect on the DPPH radicals. While in the intracellular ROS scavenging assay, the ROS generation was induced by inflammatory responses of the macrophages to the LPS stimulation. As an anti-inflammatory drug, the DEX might inhibit the generation of ROS by relieving inflammation, hence the better intracellular ROS scavenging activity of DHC NPs is owing to the synergetic effect of the anti-oxidative activity of CUR and anti-inflammatory activity of DEX.

3.7. Inflammation targeting effect of DHC NPs

As aforementioned, nanoparticles are capable of accumulation in the inflamed colon via the eEPR effect and enhanced mucosal penetration. Besides, it is worth mentioning that negatively charged nanoparticles

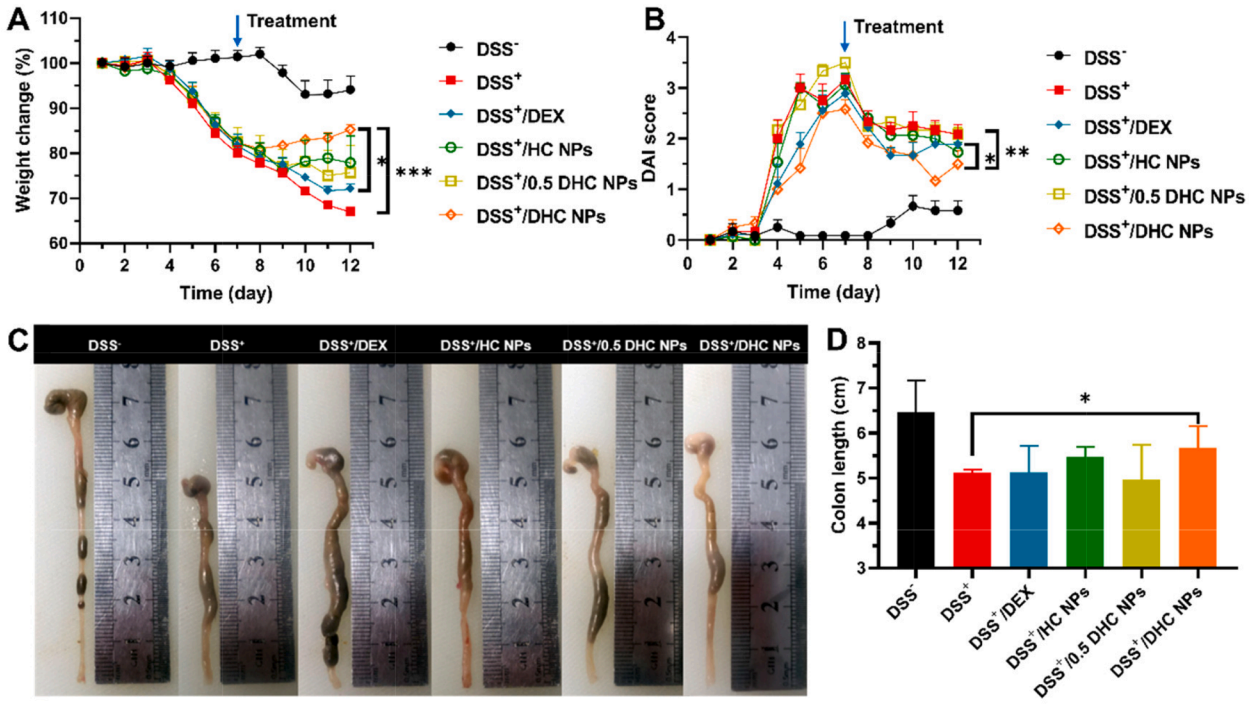

Fig. 6. *In vivo* evaluation of the therapeutic effect of DHC NPs against DDS-induced UC. (A) weight loss and (B) DAI scores of mice with different treatments. (C) Colons extracted from mice with different treatments. (D) Quantitative analysis of the colon length of mice with different treatments. $^{*}P < 0.05$, $^{**}P < 0.01$, $^{***}P < 0.005$.

are more likely to preferentially target the site of IBD because inflamed colon epithelium is positively charged due to the accumulation of positively charged proteins such as eosinophil cationic protein, transferrin, and antimicrobial peptides (Hua et al., 2015; Tirosh et al., 2009; Vafaei et al., 2016). Therefore, we hypothesized that DHC NPs with negative charges are able to target colitis. To verify this, near-infrared dye IR-780 labeled HC NPs (IHC NPs) were orally administered to mice with or without DSS-induced UC respectively, then the distribution of the IHC NPs was monitored for 24 h. Fig. 5A demonstrated the fluorescence images of mice post oral administration for 3, 10 and 24 h. It was observed that the IHC NPs were presented in the intestinal tract, and the fluorescence in mice with UC (DSS^+ group) was much stronger than that in normal mice (DSS^- group) at each time point. The fluorescence intensities at the region of interest were summarized in Fig. 5B to quantify the difference between the two groups. The mean fluorescence intensities in both groups decreased over time, whereas the fluorescence intensities in the DSS^+ group were significantly higher than that in DSS^- group at 3 and 10 h post-treatment, which was in accordance with the visible observations.

After oral administration for 24 h, the mice were sacrificed and their colons were collected and imaged. As shown in Fig. 5C, the colon of the DSS^+ group exhibited a stronger fluorescence than the colon of the DSS^- group, and the difference was significant as confirmed by the quantitative analysis (Fig. 5D). All these results verified that the HC NPs based formulations can accumulate in inflamed colon tissues and have potential for targeted drug delivery in IBD therapy.

3.8. *In vivo* therapeutic effect of DHC NPs against DSS-induced UC

In vivo therapeutic efficacy of DHC NPs against DSS-induced UC was evaluated using mice with DSS-induced UC, which was commonly used to test the efficacy of IBD therapy. UC is characterized by weight loss, diarrhea, and bloody stool, hence the body weight and a DAI calculated from the change in body weight, stool consistency, and presence of hematochezia were monitored to evaluate the severity of UC (Lin et al., 2018). A higher weight loss and DAI score indicate more severe UC.

As summarized in Fig. 6A, the bodyweight of all DSS^+ groups lost quickly during the stage of UC creation (first 7 days), indicating the successful creation of UC. Then in the following 5 days, the change in body weight of groups with different treatments exhibited the curative effect of different formulations. All groups with treatments showed a slowdown in the weight loss and even a reversion of the weight loss was observed in the group treated with high dose of DHC NPs, while the bodyweight of the DSS^+ group without treatment kept dropping down. Besides, all nanoparticles-based formulations exhibited better effect in mitigating the weight loss than free DEX. Statistical analysis indicated that the therapeutic effect at the end of the treatment of the DSS^+/DHC NPs group showed a significant difference relative to the DSS^+ group and DSS^+/DEX group. These results are unsurprising as the nanoparticles can accumulate in the colon and both CUR and DEX are beneficial in relieving inflammation. Similar results were observed in the profile of DAI scores (Fig. 6B). The DAI scores rose significantly during the DSS treatment, then dropped down in varying degrees after the administration of different formulations. Thereinto, the DAI score of the DSS^+/DHC NPs group showed a significant decrease in comparison to the DSS^+ group and DSS^+/DEX group, further proving that the DHC NPs have the best therapeutic effect against UC.

The length of the colon also reflects the pathological degree of colitis because scarring of the inflamed site will shorten the colon (Nowarski et al., 2015). After treatment, the mice were sacrificed and the length of colons was measured. As displayed in Fig. 6C, the DSS treatment significantly shorten the colon relative to the untreated group. However, treatment with DEX or nanoparticle formulations preserved the length of the colon. The DSS^+ group had the shortest average colon length of 5.1 cm, relative to 6.6 cm of the DSS^- group, while the average colon length of the DSS^+/DEX, DSS^+/HC NPs, DSS^+/0.5 DHC NPs, DSS^+/ DHC NPs was 5.1 cm, 5.5 cm, 5.0 cm, and 5.7 cm respectively (Fig. 6D). Further analysis manifested that the colon length of the DHC NPs treated group showed significant differences relative to the DSS^+ group, indicating that the scarring-induced shortening of the colon can be ameliorated by oral administration of DHC NPs.

Subsequently, the colon sections from each group were examined to

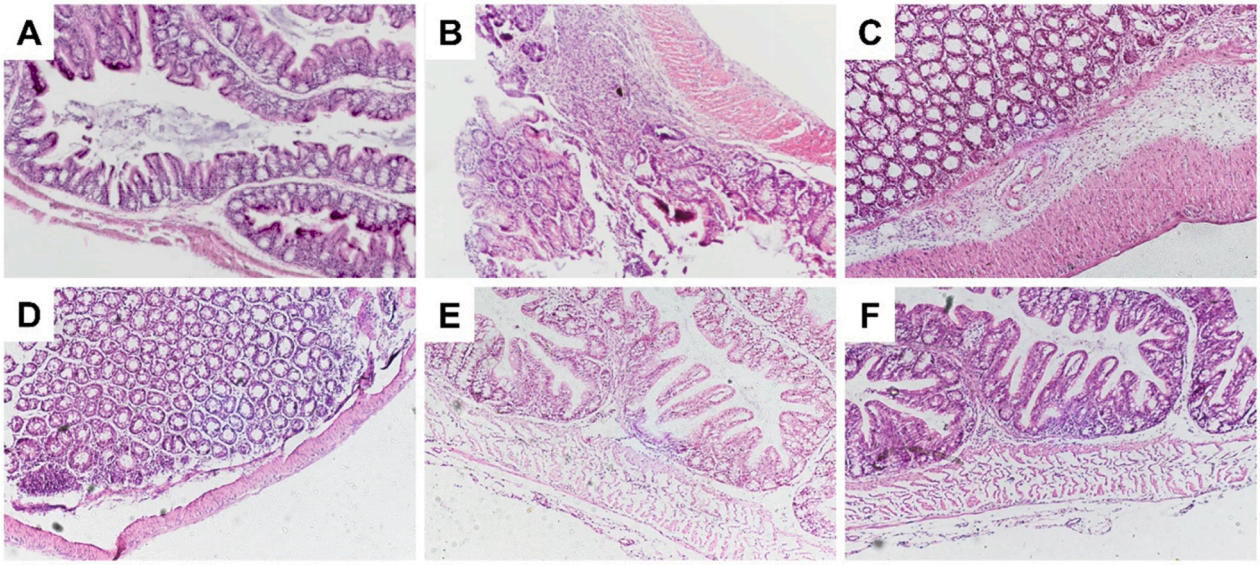

Fig. 7. Representative images of H&E stained colon sections from various groups. (A) DSS^- group, (B) DSS^+ group, (C) DSS^+/DEX group, (D) DSS^+/HC NPs group, (E) DSS^+/0.5 DHC NPs group, (F) DSS^+/ DHC NPs group. Thickness: 5 μm. Images of tissues are shown at 100 × magnification.

analyze the pathological lesions. The H&E-stained colon sections were shown in Fig. 7, which directly reflected the degree of lesions in the colons. In addition to obvious interstitial edema and dramatic loss of goblet cells, the colon section of DSS-treated mice exhibited massive destruction of entire epithelial, accompanied with a changed mucosa structure, indicating the severity of DSS-induced UC. Compared with the DSS^+ group, the free DEX and HC NPs helped to improve the structure of intestinal mucosa slightly. Encouragingly, the ulceration and edema induced by DSS were fade away in the colon of mice treated with DHC NPs, and nearly the same morphological structures were observed between DSS^+/ DHC NPs and DSS^- group. These histological findings confirmed that DHC NPs treatment is beneficial to alleviate inflammatory lesions caused by the DSS-induced UC. Overall, these results revealed that the DHC NPs with the merits of eEPR-mediated targeting and combined treatment are promising candidates for improved IBD therapy.

4. Conclusion

In summary, we prepared an oral nanoparticle formulation (DHC NPs) simultaneously loaded with an anti-inflammatory drug and ROS scavenger by encapsulating anti-inflammatory drug DEX into nanoparticles formed by self-assembly of HES-CUR conjugates. The DHC NPs can keep stable in the harsh gastric environment and release loaded therapeutics in an α-amylase-responsive manner due to the degradation of HES in the environment of the inflamed colon. Since the vehicles consist of food-derived compounds, the DHC NPs are highly biocompatible with macrophages. Besides, the DHC NPs show excellent intracellular ROS scavenging activity after being effectively internalized via endocytosis. Benefiting from the nanoscale size and negative charge, the DHC NPs can accumulate in the inflamed site of the colon *via* the eEPR effect and interaction with the positively charged epithelium in the inflamed colon. The *in vivo* evaluation of therapeutic effect against DSS-induced UC in mice revealed that the DHC NPs can enhance the efficacy of free DEX and significantly relieve the lesion caused by UC. Incorporating the merits of targeted drug delivery and combined therapy with an anti-inflammatory drug and ROS scavenger, the DHC NPs hold great potential in developing novel oral formulations for advanced IBD therapy.

CRediT authorship contribution statement

Chenlan Xu: Methodology, Investigation, Writing – original draft. **Shuting Chen:** Methodology, Investigation. **Cuiping Chen:** Methodology, Investigation. **Yangcan Ming:** Methodology, Validation. **Jiahao Du:** Investigation. **Jinyi Mu:** Investigation. **Fang Luo:** Methodology. **Da Huang:** Conceptualization, Writing – review & editing. **Na Wang:** Conceptualization, Writing – review & editing. **Zhenyu Lin:** Resources. **Zuquan Weng:** Supervision, Writing – review & editing.

Declaration of Competing Interest

The authors declare that they have no known competing financial interests or personal relationships that could have appeared to influence the work reported in this paper.

Acknowledgments

The authors would like to thank Dr. Guixuan Zhou for the assistance in animal experiments and financial support from the National Natural Science Foundation of China (81971837), the Natural Science Foundation of Fujian Province (2019J05031), the Natural Science Foundation of Hubei Province (2019CFB401), and the Foundation for Scholars of Fuzhou University (XRC-17044).

Appendix A. Supplementary material

Supplementary data to this article can be found online at https://doi.org/10.1016/j.ijpharm.2022.121884.

References

Abraham, C., Cho, J.H., 2009. Inflammatory bowel disease. New Engl. J. Med. 361 (21), 2066–2078.
Guan, Q., 2019. A comprehensive review and update on the pathogenesis of inflammatory bowel disease. J. Immunol. Res. 2019, 7247238.
Ng, S.C., Shi, H.Y., Hamidi, N., Underwood, F.E., Tang, W., Benchimol, E.I., Panaccione, R., Ghosh, S., Wu, J.C.Y., Chan, F.K.L., Sung, J.J.Y., Kaplan, G.G., 2017. Worldwide incidence and prevalence of inflammatory bowel disease in the 21st century: a systematic review of population-based studies. Lancet 390 (10114), 2769–2778.
Kotla, N.G., Rana, S., Sivaraman, G., Sunnapu, O., Vemula, P.K., Pandit, A., Rochev, Y., 2018. Bioresponsive drug delivery systems in intestinal inflammation: state-of-the-art and future perspectives. Adv. Drug Delivery Rev. 146, 248–266.

Graham, D.B., Xavier, R.J., 2020. Pathway paradigms revealed from the genetics of inflammatory bowel disease. Nature 578 (7796), 527–539.
Jeong, D.Y., Kim, S., Son, M.J., Son, C.Y., Kim, J.Y., Kronbichler, A., Lee, K.H., Shin, J.I., 2019. Induction and maintenance treatment of inflammatory bowel disease: a comprehensive review. Autoimmun. Rev. 18 (5), 439–454.
Seshadri, S., Pope, R.L., Zenewicz, L.A., 2018. Glucocorticoids inhibit group 3 innate lymphocyte il-22 production. J. Immunol. 201 (4), 1267–1274.
Sood, A., Midha, V., Sood, N., Awasthi, G., 2002. A prospective, open-label trial assessing dexamethasone pulse therapy in moderate to severe ulcerative colitis. J. Clin. Gastroenterol 35 (4), 328–331.
Kesharwani, S.S., Ahmad, R., Bakkari, M.A., Rajput, M.K.S., Dachineni, R., Valiveti, C.K., Kapur, S., Jayarama Bhat, G., Singh, A.B., Tummala, H., 2018. Site-directed non-covalent polymer-drug complexes for inflammatory bowel disease (IBD): Formulation development, characterization and pharmacological evaluation. J. Controlled Release 290, 165–179.
Zai, K., Hirota, M., Yamada, T., Ishihara, N., Mori, T., Kishimura, A., Suzuki, K., Hase, K., Katayama, Y., 2018. Therapeutic effect of vitamin D3-containing nanostructured lipid carriers on inflammatory bowel disease. J. Controlled Release 286, 94–102.
Dou, Y., Li, C., Li, L., Guo, J., Zhang, J., 2020. Bioresponsive drug delivery systems for the treatment of inflammatory diseases. J. Controlled Release 327, 641–666.
Nguyen, T.-H.-T., Trinh, N.-T., Tran, H.N., Tran, H.T., Le, P.Q., Ngo, D.-N., Tran-Van, H., Van Vo, T., Vong, L.B., Nagasaki, Y., 2021. Improving silymarin oral bioavailability using silica-installed redox nanoparticle to suppress inflammatory bowel disease. J. Controlled Release 331, 515–524.
Gou, S., Huang, Y., Wan, Y., Ma, Y., Zhou, X., Tong, X., Huang, J., Kang, Y., Pan, G., Dai, F., Xiao, B., 2019. Multi-bioresponsive silk fibroin-based nanoparticles with on-demand cytoplasmic drug release capacity for CD44-targeted alleviation of ulcerative colitis. Biomaterials 212, 39–54.
Le, Z., He, Z., Liu, H., Liu, L., Liu, Z., Chen, Y., 2021. Antioxidant enzymes sequestered within lipid–polymer hybrid nanoparticles for the local treatment of inflammatory bowel disease. ACS Appl. Mater. Interfaces 13 (47), 55966–55977.
Bertoni, S., Liu, Z., Correia, A., Martins, J.P., Rahikkala, A., Fontana, F., Kemell, M., Liu, D., Albertini, B., Passerini, N., Li, W., Santos, H.A., 2018. pH and reactive oxygen species-sequential responsive nano-in-micro composite for targeted therapy of inflammatory bowel disease. Adv. Funct. Mater. 28 (50), 1806175.
Hua, S., Marks, E., Schneider, J.J., Keely, S., 2015. Advances in oral nano-delivery systems for colon targeted drug delivery in inflammatory bowel disease: selective targeting to diseased versus healthy tissue. Nanomedicine 11 (5), 1117–1132.
Zhang, J., Zhao, Y., Hou, T., Zeng, H., Kalambhe, D., Wang, B., Shen, X., Huang, Y., 2020. Macrophage-based nanotherapeutic strategies in ulcerative colitis. J. Controlled Release 320, 363–380.
Fousekis, F.S., Theopistos, V.I., Katsanos, K.H., Christodoulou, D.K., 2018. Pancreatic involvement in inflammatory bowel disease: a review. J. Clin. Med. Res. 10 (10), 743–751.
Castangia, I., Nácher, A., Caddeo, C., Merino, V., Díez-Sales, O., Catalán-Latorre, A., Fernàndez-Busquets, X., Fadda, A.M., Manconi, M., 2015. Manconi, Therapeutic efficacy of quercetin enzyme-responsive nanovesicles for the treatment of experimental colitis in rats. Acta Biomater. 13, 216–227.
Ali, H., Weigmann, B., Neurath, M.F., Collnot, E.M., Windbergs, M., Lehr, C.M., 2014. Budesonide loaded nanoparticles with pH-sensitive coating for improved mucosal targeting in mouse models of inflammatory bowel diseases. J. Controlled Release 183, 167–177.
Wang, X., Yan, J.-J., Wang, L., Pan, D., Yang, R., Xu, Y., Sheng, J., Huang, Q., Zhao, H., Yang, M., 2018. Rational design of polyphenol-poloxamer nanovesicles for targeting inflammatory bowel disease therapy. Chem. Mater. 30 (12), 4073–4080.
Debnath, T., Kim, D.H., Lim, B.O., 2013. Natural products as a source of anti-inflammatory agents associated with inflammatory bowel disease. Molecules 18 (6), 7253–7270.
Liu, Y., Cheng, Y., Zhang, H., Zhou, M., Yu, Y., Lin, S., Jiang, B., Zhao, X., Miao, L., Wei, C.-W., Liu, Q., Lin, Y.-W., Du, Y., Butch, C.J., Wei, H., 2020. Integrated cascade nanozyme catalyzes in vivo ROS scavenging for anti-inflammatory therapy. Sci. Adv. 6 (29), eabb2695.
Vecchi Brumatti, L., Marcuzzi, A., Tricarico, P.M., Zanin, V., Girardelli, M., Bianco, A.M., 2014. Curcumin and inflammatory bowel disease: potential and limits of innovative treatments. Molecules 19 (12), 21127–21153.
Gao, X., Xu, Z., Liu, G., Wu, J., 2021. Polyphenols as a versatile component in tissue engineering. Acta Biomater. 119, 57–74.
Friedrich, M., Pohin, M., Powrie, F., 2019. Cytokine networks in the pathophysiology of inflammatory bowel disease. Immunity 50 (4), 992–1006.
Kunnumakkara, A.B., Anand, P., Aggarwal, B.B., 2008. Curcumin inhibits proliferation, invasion, angiogenesis and metastasis of different cancers through interaction with multiple cell signaling proteins. Cancer Lett. 269 (2), 199–225.
Pluta, R., Januszewski, S., Ułamek-Kozioł, M., 2020. Mutual two-way interactions of curcumin and gut microbiota. Int. J. Mol. Sci. 21 (3), 1055.
Hassaninasab, A., Hashimoto, Y., Tomita-Yokotani, K., Kobayashi, M., 2011. Discovery of the curcumin metabolic pathway involving a unique enzyme in an intestinal microorganism. Proc. Natl. Acad. Sci. U. S. A. 108 (16), 6615–6620.
Deguchi, Y., Andoh, A., Inatomi, O., Yagi, Y., Bamba, S., Araki, Y., Hata, K., Tsujikawa, T., Fujiyama, Y., 2007. Curcumin prevents the development of dextran sulfate sodium (DSS)-induced experimental colitis. Digest. Dis. Sci. 52 (11), 2993–2998.
Chen, S., Wu, J., Tang, Q., Xu, C., Huang, Y., Huang, D., Luo, F., Wu, Y., Yan, F., Weng, Z., Wang, S., 2020. Nano-micelles based on hydroxyethyl starch-curcumin conjugates for improved stability, antioxidant and anticancer activity of curcumin. Carbohydr. Polym. 228, 115398.
Camilleri, M., Colemont, L.J., Phillips, S.F., Brown, M.L., Thomforde, G.M., Chapman, N., Zinsmeister, A.R., 1989. Human gastric emptying and colonic filling of solids characterized by a new method. Am. J. Physiol. 257 (2), G284–G290.
O'Toole, M.G., Soucy, P.A., Chauhan, R., Raju, M.V.R., Patel, D.N., Nunn, B.M., Keynton, M.A., Ehringer, W.D., Nantz, M.H., Keynton, R.S., Gobin, A.S., 2016. Release-modulated antioxidant activity of a composite curcumin-chitosan polymer. Biomacromolecules 17 (4), 1253–1260.
Cunha Neto, F., Marton, L.T., de Marqui, S.V., Lima, T.A., Barbalho, S.M., 2019. Curcuminoids from curcuma longa: new adjuvants for the treatment of crohn's disease and ulcerative colitis? Crit. Rev. Food Sci. 59 (13), 2136–2143.
Burge, K., Gunasekaran, A., Eckert, J., Chaaban, H., 2019. Curcumin and intestinal inflammatory diseases: molecular mechanisms of protection. Int. J. Mol. Sci. 20 (8), 1912.
Paleos, C.M., Sideratou, Z., Tsiourvas, D., 2017. Drug delivery systems based on hydroxyethyl starch. Bioconjugate Chem. 28 (6), 1611–1624.
Hu, H., Li, Y., Zhou, Q., Ao, Y., Yu, C., Wan, Y., Xu, H., Li, Z., Yang, X., 2016. Redox-sensitive hydroxyethyl starch-doxorubicin conjugate for tumor targeted drug delivery. ACS Appl. Mater. Interfaces 8 (45), 30833–30844.
Tirosh, B., Khatib, N., Barenholz, Y., Nissan, A., Rubinstein, A., 2009. Transferrin as a luminal target for negatively charged liposomes in the inflamed colonic mucosa. Mol. Pharmaceutics 6 (4), 1083–1091.
Vafaei, S.Y., Esmaeili, M., Amini, M., Atyabi, F., Ostad, S.N., Dinarvand, R., 2016. Self assembled hyaluronic acid nanoparticles as a potential carrier for targeting the inflamed intestinal mucosa. Carbohydr. Polym. 144, 371–381.
Lin, W.C., Pan, W.Y., Liu, C.K., Huang, W.X., Song, H.L., Chang, K.S., Li, M.J., Sung, H. W., 2018. In situ self-spray coating system that can uniformly disperse a poorly water-soluble H_2S donor on the colorectal surface to treat inflammatory bowel diseases. Biomaterials 182, 289–298.
Nowarski, R., Jackson, R., Gagliani, N., de Zoete, M.R., Palm, N.W., Bailis, W., Low, J.S., Harman, C.C.D., Graham, M., Elinav, E., Flavell, R.A., 2015. Epithelial IL-18 equilibrium controls barrier function in colitis. Cell 163 (6), 1444–1456.